Cell Metabolism
Article

Angptl4 Protects against Severe Proinflammatory Effects of Saturated Fat by Inhibiting Fatty Acid Uptake into Mesenteric Lymph Node Macrophages

Laeticia Lichtenstein,[1,2,9] Frits Mattijssen,[2,9] Nicole J. de Wit,[1,2,9] Anastasia Georgiadi,[2] Guido J. Hooiveld,[1,2] Roelof van der Meer,[1,2,3] Yin He,[4] Ling Qi,[5] Anja Köster,[6] Jouke T. Tamsma,[7] Nguan Soon Tan,[8] Michael Müller,[1,2] and Sander Kersten[1,2,5,*]

[1]Nutrigenomics Consortium, TI Food and Nutrition, 6700AN, Wageningen, The Netherlands
[2]Nutrition, Metabolism, and Genomics group, Division of Human Nutrition, Wageningen University, 6700EV, Wageningen, The Netherlands
[3]NIZO Food Research, 6710BA, Ede, The Netherlands
[4]Graduate Program in Genetics and Development
[5]Division of Nutritional Sciences
Cornell University, Ithaca, NY 14853, USA
[6]Lilly Research Laboratories, Eli Lilly and Company, Indianapolis, IN 46225, USA
[7]Department of General Internal Medicine and Endocrinology, Leiden University Medical Centre, 2300RC, Leiden, The Netherlands
[8]School of Biological Sciences, Nanyang Technological University, Singapore 637551, Singapore
[9]These authors contributed equally to this work
*Correspondence: sander.kersten@wur.nl
DOI 10.1016/j.cmet.2010.11.002

SUMMARY

Dietary saturated fat is linked to numerous chronic diseases, including cardiovascular disease. Here we study the role of the lipoprotein lipase inhibitor Angptl4 in the response to dietary saturated fat. Strikingly, in mice lacking Angptl4, saturated fat induces a severe and lethal phenotype characterized by fibrinopurulent peritonitis, ascites, intestinal fibrosis, and cachexia. These abnormalities are preceded by a massive acute phase response induced by saturated but not unsaturated fat or medium-chain fat, originating in mesenteric lymph nodes (MLNs). MLNs undergo dramatic expansion and contain numerous lipid-laden macrophages. In peritoneal macrophages incubated with chyle, Angptl4 dramatically reduced foam cell formation, inflammatory gene expression, and chyle-induced activation of ER stress. Induction of macrophage Angptl4 by fatty acids is part of a mechanism that serves to reduce postprandial lipid uptake from chyle into MLN-resident macrophages by inhibiting triglyceride hydrolysis, thereby preventing macrophage activation and foam cell formation and protecting against progressive, uncontrolled saturated fat-induced inflammation.

INTRODUCTION

Studies indicate that elevated saturated fat consumption is associated with increased risk for chronic diseases, including cardiovascular disease and type 2 diabetes. However, the underlying mechanisms and why specifically saturated fat is harmful largely remain unknown. Consequently, there is a need to better understand the molecular mechanisms that govern the response to dietary (saturated) fat ingestion.

After digestion of dietary fat, absorbed long-chain fatty acids are incorporated into chylomicrons as triglycerides (TG) and released into the circulation after passage through the intestinal lymphatics. Hydrolysis of chylomicron-TG is catalyzed by the enzyme lipoprotein lipase (LPL), which is anchored to the capillary endothelium via heparin-sulfate proteoglycans and is a key determinant of cellular fatty acid uptake (Merkel et al., 2002). LPL is expressed at high levels in tissues that depend on fatty acids as fuel (heart, skeletal muscle) or synthesize fats for storage or secretion (adipose tissue, mammary tissue), but high expression is also found in macrophages (Ostlund-Lindqvist et al., 1983; Wang and Eckel, 2009).

Activity of LPL is governed via numerous mechanisms that act primarily at the posttranscriptional and posttranslational level. One important modulator of LPL activity is Angiopoietin-like protein 4 (Angptl4) (Yoshida et al., 2002). Angptl4 was discovered as a transcriptional target of the peroxisome proliferator-activated receptor α and γ and is expressed in numerous cell types including adipocytes, hepatocytes, (cardio)myocytes, and endothelial cells (Kersten et al., 2000; Yoon et al., 2000). Studies using different transgenic mouse models of Angptl4 overexpression or deletion show that Angptl4 potently raises plasma TG levels by suppressing LPL-mediated clearance of plasma TG-rich lipoproteins (Koster et al., 2005; Mandard et al., 2006; Xu et al., 2005).

Recently it was shown that deletion of other members of the Angiopoietin-like protein family influences the development of obesity-related complications in the C57Bl/6 mouse high-fat-induced obesity model. Specifically, surviving *Angptl6*$^{-/-}$ mice developed marked obesity, ectopic fat storage, and insulin resistance. In contrast, mice overexpressing Angptl6 were leaner and had improved insulin sensitivity (Oike et al., 2005). Deletion of Angptl2 ameliorated adipose tissue inflammation and insulin resistance in obese mice, whereas Angptl2 overexpression

promoted adipose tissue inflammation and systemic insulin resistance (Tabata et al., 2009). Given the role of Angptl4 in plasma clearance of dietary TG, we set out to study the effect of Angptl4 deletion in the context of chronically elevated dietary fat intake.

RESULTS

Angptl4$^{-/-}$ Mice Fed HFD Develop Fibrinopurulent Peritonitis and Ascites

To examine the effect of Angptl4 on diet-induced obesity and its metabolic consequences, wild-type (WT) and *Angptl4*$^{-/-}$ mice were fed a high-fat diet (HFD) containing saturated fat-rich palm oil and compared with mice fed a low-fat diet (LFD) (see Table S1 available online). As expected based on its ability to inhibit LPL, *Angptl4*$^{-/-}$ mice had decreased plasma TG (Figure 1A) and showed faster initial weight gain (Figure 1B) (Voshol et al., 2009). Remarkably, bodyweights of *Angptl4*$^{-/-}$ mice fed HFD reached a plateau after around 12 weeks and declined thereafter (Figure 1B). The decrease in bodyweight was related to anorexia noticeable after about 10 weeks of HFD (Figure 1C). All *Angptl4*$^{-/-}$ mice fed HFD ultimately die anywhere between 15 and 25 weeks. The cause of death was identified by an animal pathologist as severe fibrinopurulent peritonitis connected with ascites.

Large amounts of fibrin exudate covered the abdominal organs in *Angptl4*$^{-/-}$ mice fed a HFD (Figure 1D). Other macroscopic abnormalities included intestinal fibrosis (Figure 1E), a compressed liver (Figure S1A), and a hyperplastic spleen (data not shown). No such abnormalities were observed in *Angptl4*$^{-/-}$ mice fed LFD, even at high age (>1.5 years). Routine clinical tests were performed on the ascites fluid, which varied in color from purulent white to purulent red (Figure 1D, inset). Ascites white blood cell count was extremely high in all animals (25.5–34.1*10^9/L, diagnostic threshold <0.5*10^9/L), as was the endotoxin concentration (50–120 EU/mL, zero threshold), strongly suggesting bacterial peritonitis. Ascites fluid of some animals tested positive for *E. coli*. The high protein concentration (3.43–4.28 g/dL, diagnostic threshold >2.5 g/dL) and low serum-ascites albumin gradient (SAAG, 0.11–0.34 g/dL, diagnostic threshold <1.1 g/dL) indicated exudative ascites, thereby excluding portal hypertension. The ascites TG concentration was highly variable but clearly elevated (4.8–75.5 mM, diagnostic threshold ~1.25 mM). Analysis of chylous ascites fluid by lipoprotein profiling indicated an abundance of TG-rich lipoproteins representing chylomicrons, as shown by immunostaining for apoB (Figure 1F), suggesting leakage of chyle from lymphatic vessels. Additionally, significant vascular leakage occurred, as shown by the much lower protein concentration in chyle (1.38–1.83 g/dL) compared to ascites fluid (3.43–4.28 g/dL).

Plasma endotoxin levels were significantly elevated in *Angptl4*$^{-/-}$ mice fed HFD for 19 weeks (Figure 1G). Microscopic examination indicated that the fibrin exudate contained an abundance of foam cells, polynuclear giant cells, and other leukocytes (data not shown). The same cells as well as focal lymphocyte infiltrates were observed in the small intestine (Figure 2A, inset) and mesenteric fat (Figure 2B), in the former encapsulated by collagen (Figure 2C). Intestinal lymph vessels were dilated, suggesting mesenteric lymphatic obstruction (Figure 1H). Epididymal adipose tissue had a red appearance (Figure S1C) and exhibited coagulation necrosis and steatitis as shown by presence of lymphocytes, granulocytes, and other leukocytes (Figure S1D, inset).

Livers of *Angptl4*$^{-/-}$ mice fed HFD for 19 weeks were not fibrotic but resembled an ischemic liver. Portal triads, cords, and sinusoids were poorly visible, and clumping of nuclei was seen, indicating collapse of liver (Figures S1A and S1B). Focal infiltrates of neutrophils, eosinophils, and macrophages were observed (Figure S1B, inset), as were rod-shaped bacteria. Liver fat was almost absent, whereas it was elevated in *Angptl4*$^{-/-}$ mice on LFD (Figure S1E). Weights of liver and epididymal fat pads were significantly lower in *Angptl4*$^{-/-}$ mice after 19 weeks of HFD (Figures S1F and S1G), while epididymal fat pads were heavier in *Angptl4*$^{-/-}$ mice on the LFD. Taken together, *Angptl4*$^{-/-}$ mice chronically fed HFD develop a severe phenotype characterized by anorexia, cachexia, intestinal inflammation and fibrosis, chylous ascites, and fibrinopurulent peritonitis, leading to the death of the animal.

Ascites and Other Clinical Abnormalities Are Not Related to a Primary Lymph Vessel Defect

Angptl4$^{-/-}$ mice on a mixed genetic background were reported to die shortly after birth due to defective separation of intestinal lymphatic and blood microvasculature (Backhed et al., 2007). Although we did not find these abnormalities in *Angptl4*$^{-/-}$ mice on pure C57Bl/6 background and adult *Angptl4*$^{-/-}$ mice in proper Mendelian ratios were obtained, one might suspect an underlying primary weakness in intestinal lymphatics that becomes manifest when chyle flow is increased, as observed upon high-fat feeding, causing leakage of chyle into intestinal lumen and peritoneal cavity. However, none of the clinical abnormalities including chylous ascites were observed in *Angptl4*$^{-/-}$ mice fed a safflower oil-based HFD rich in polyunsaturated fat (Table S2) (data not shown). Furthermore, if lymphatic vessels are intrinsically more permeable, ascites and diarrhea, the latter due to loss of protein and fat from lymph into the intestinal lumen, should develop upon starting the HFD, which was not observed. Surprisingly, fecal fat excretion was markedly decreased in *Angptl4*$^{-/-}$ mice, indicating more efficient fat absorption (Figure S2A). An acute intestinal lipid absorption test using ^{3}H-triolein and ^{14}C-palmitic acid failed to show any differences in rate of appearance of either label in blood between WT and *Angptl4*$^{-/-}$ mice (Figures S2B and S2C), suggesting chylomicron formation and release is similar between WT and *Angptl4*$^{-/-}$ mice. In contrast, in all intestinal parts, accumulation of both labels 5 hr after lipid load was markedly higher in *Angptl4*$^{-/-}$ mice (Figures S2D and S2E). The similarity in results between ^{3}H-triolein and ^{14}C-palmitic acid argue against an effect of Angptl4 inactivation on TG digestion but suggest enhanced fatty acid uptake into enterocytes. This is supported by elevated expression of target genes of PPARα in small intestine of *Angptl4*$^{-/-}$ mice, suggesting enhanced gene regulation by fatty acids (Figures S2F and S2G). Overall, the data argue against a primary lymph vessel defect forming the basis for the severe pathology.

A Massive Acute Phase Response Precedes Ascites in *Angptl4*$^{-/-}$ Mice Fed HFD

To investigate the cause of the severe pathology, WT and *Angptl4*$^{-/-}$ mice were studied before onset of anorexia and cachexia at 8 weeks of HFD (Figures 1A and 1B), and before

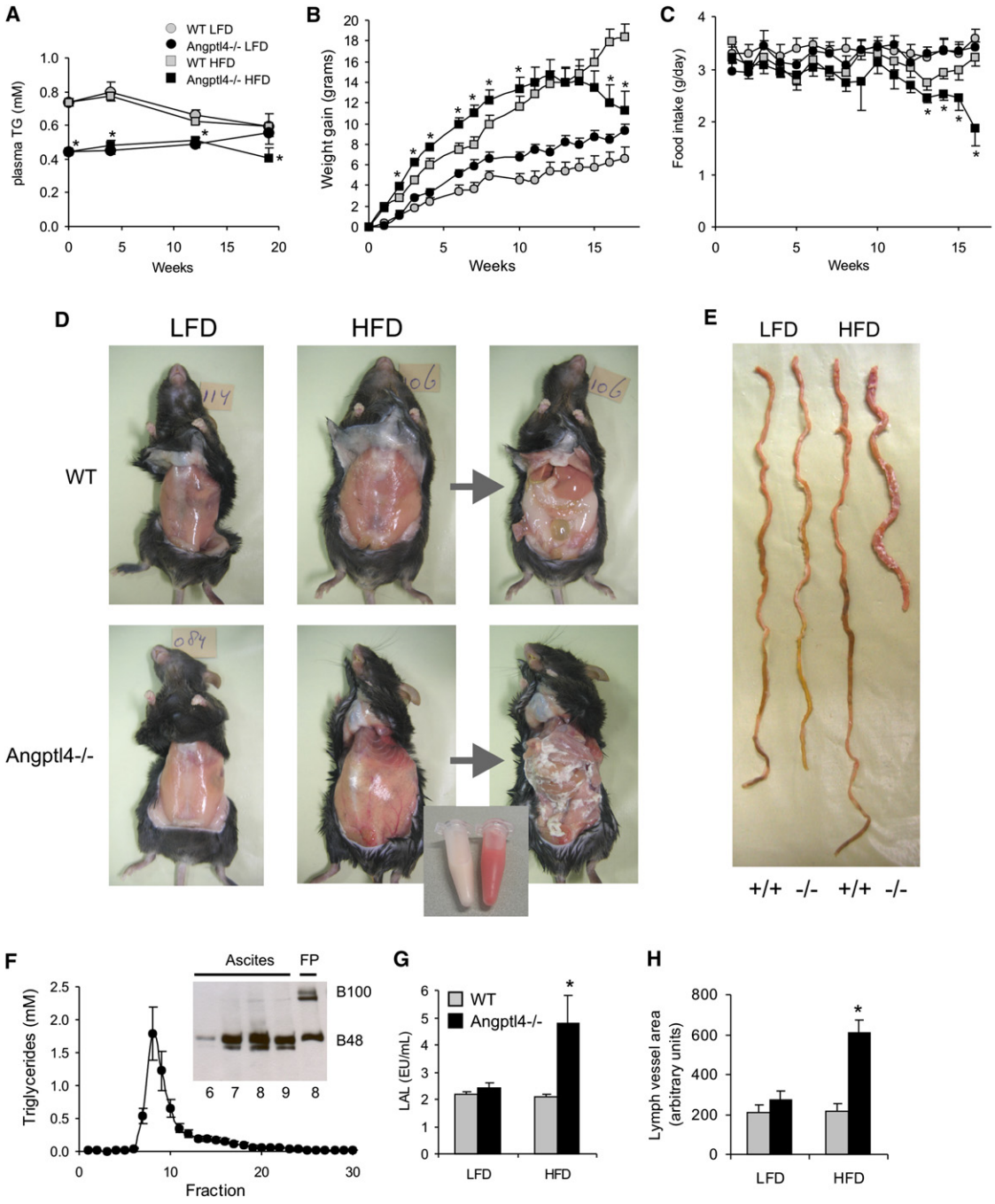

Figure 1. *Angptl4*$^{-/-}$ Mice Chronically Fed HFD Develop Fibrinopurulent Peritonitis and Ascites

(A) Four hour fasting plasma TG levels during the course of chronic LFD or HFD intervention (study 1). Differences between LFD and HFD within each genotype were not statistically significant. n = 10 per group.

(B) Bodyweight changes in WT and *Angptl4*$^{-/-}$ mice fed LFD or HFD for 19 weeks.

(C) Mean daily food intake in WT and *Angptl4*$^{-/-}$ mice fed LFD or HFD for 19 weeks.

(D) Whole-animal photographs taken immediately following sacrifice of representative WT and *Angptl4*$^{-/-}$ mice fed either LFD or HFD for 19 weeks. Pictures at far right were taken after removal of peritoneum. Ascites fluid collected from two *Angptl4*$^{-/-}$ mice fed HFD is shown at the bottom.

(E) Photograph of small intestine of WT and *Angptl4*$^{-/-}$ mice fed LFD or HFD for 19 weeks.

(F) FLPC lipoprotein profiling of ascites fluid of *Angptl4*$^{-/-}$ mice fed HFD for 19 weeks (n = 5). (Inset) apoB immunoblot of FPLC fractions from ascites fluid of *Angptl4*$^{-/-}$ mice or mouse fasting plasma (FP).

(G) Plasma endotoxin levels in WT and *Angptl4*$^{-/-}$ mice fed LFD or HFD for 19 weeks.

(H) Lymph vessel area in jejunum of WT and *Angptl4*$^{-/-}$ mice fed LFD or HFD for 19 weeks determined after Lyve-1 staining. Error bars represent SEM. Asterisk indicates significantly different from corresponding WT mice according to Student's t test ($p < 0.05$).

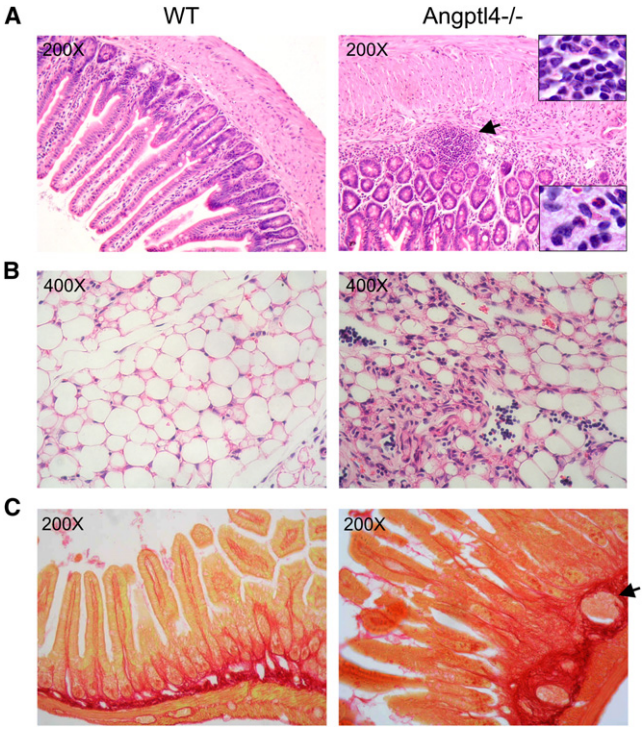

Figure 2. Severe Intestinal Inflammation in Angptl4$^{-/-}$ Mice Chronically Fed HFD

Representative H&E staining of small intestine (A) or mesenteric fat (B) of WT and *Angptl4*$^{-/-}$ mice fed HFD for 19 weeks (study 1). (Inset) High-magnification image of lymphocyte infiltrate (top) or presence of granulocytes (bottom). (C) Sirius red staining of small intestine of WT and *Angptl4*$^{-/-}$ mice fed HFD for 19 weeks. Arrow indicates inflammatory infiltrate.

ascites or other macroscopic abnormalities were observed. Strikingly, after 8 weeks of HFD, plasma levels of serum amyloid A (SAA) and other inflammatory markers were dramatically increased in *Angptl4*$^{-/-}$ mice (Figures 3A and 3B). Whereas IL-6 was undetectable in plasma of WT mice, levels averaged 63 ± 26 pg/mL in *Angptl4*$^{-/-}$ mice (normal values <15 pg/mL). These changes were paralleled by massive induction of hepatic mRNA for SAA2 and other acute phase proteins haptoglobin and lipocalin 2 (Figure 3C). Furthermore, increased expression of macrophage/Kupffer cell marker Cd68 (Figure 3D) and enhanced Cd68 immunostaining was observed (Figure 3E). Consistent with these data, serum levels of negative acute phase protein albumin were decreased (Figure 3F). Thus, *Angptl4*$^{-/-}$ mice fed HFD exhibit systemic inflammation and a massive acute phase response several weeks prior to development of ascites and other clinical symptoms.

Chronic HFD is known to induce adipose tissue inflammation, characterized by adipose infiltration of macrophages. However, no signs of enhanced macrophage or other leukocyte infiltration were observed in epididymal fat of *Angptl4*$^{-/-}$ mice after 8 weeks of HFD (Figures S3A and S3B), suggesting that enhanced systemic inflammation does not originate in the adipose tissue.

Inflammation in *Angptl4*$^{-/-}$ Mice Fed HFD Originates in Mesenteric Lymph Nodes

Interestingly, a trend toward increased plasma SAA levels in *Angptl4*$^{-/-}$ mice was already visible after 1 week of HFD (Figure 4A). HFD has been proposed to lead to inflammatory stress via changes in intestinal microflora and/or increased release of LPS (Cani et al., 2007). However, portal LPS levels were lowest in *Angptl4*$^{-/-}$ mice fed HFD (Figure 4B). Importantly, the increase in plasma SAA levels in *Angptl4*$^{-/-}$ mice by HFD was unaffected by chronic oral antibiotic treatment (Figure 4C), which effectively reduced intestinal bacterial counts (Figure 4D, Figure S4A) and resulted in a severely enlarged caecum (data not shown). These data suggest that induction of systemic inflammation in *Angptl4*$^{-/-}$ mice by HFD is independent of the intestinal microbiota.

Remarkably, we noticed that the mesenteric lymph nodes (MLNs) were dramatically enlarged in *Angptl4*$^{-/-}$ mice already after 5 weeks of HFD, indicating massive mesenteric lymphadenitis (Figures 4E and 4F). Inflammation extended to mesenteric fat which exhibited mesenteric panniculitis (Figure S4B). High-fat feeding is known to promote intestinal lymph flow and formation of chylomicrons, which pass through the MLN as chyle before reaching the circulation. Hence, MLN are exposed to extremely high TG concentrations, which reach 55 mM in rats fed HFD (mean 35 ± 11 mM). To investigate the role of increased chyle flow, mice were fed for 5 weeks a diet rich in medium chain TGs (MCT) (Table S2), which are not processed via the lymph but enter the portal vein as free fatty acids. Remarkably, induction of plasma SAA and mesenteric lymphadenitis were absent in *Angptl4*$^{-/-}$ mice fed MCT (Figures 4G and 4H), suggesting the response is mediated by chylomicrons. A safflower oil-based HFD, which as mentioned previously did not provoke a clinical phenotype, also did not promote inflammation in *Angptl4*$^{-/-}$ mice, whereas a lard-based high saturated fat diet gave similar results as the palm-oil based HFD (Figures 4G and 4H). Use of a palm oil-based diet with intermediate fat content supported a clear correlation between dietary saturated fat content and plasma SAA in *Angptl4*$^{-/-}$ mice (Figure 4I). Consistent with a direct proinflammatory effect of saturated fat via chylomicrons, there was a clear trend toward increased expression of several inflammatory mediators in MLN of *Angptl4*$^{-/-}$ mice already after 1 day of HFD (Figure 4J, Figure S4C). These data indicate that in *Angptl4*$^{-/-}$ mice, a diet rich in saturated fat rapidly causes severe mesenteric lymphadenitis and panniculitis via chylomicrons, leading to a massive hepatic acute phase response via the connecting portal circulation.

Absence of Angptl4 Stimulates Foam Cell Formation and Inflammation in MLN Macrophages

MLNs are packed with numerous immune cells including macrophages. Microscopic examination of MLN from *Angptl4*$^{-/-}$ mice but not WT mice fed HFD for 5 weeks showed an abundance of multinucleated Touton giant cells (Figures 5A and 5B), originating from fusion of aberrant lipid-laden tissue macrophages as verified by F4/80 immunostaining (Figure 5C). Formation of Touton cells is known to occur as reaction to lipid material in lymph nodes and is characteristic of lipid lymphadenopathy (Aterman et al., 1988). Accumulation of neutral lipids in Touton cells was confirmed by oil red O (Figure 5D) and Sudan black staining (Figure 5E). Importantly, Touton cells were spotted in *Angptl4*$^{-/-}$ mice already after 1 day of HFD (Figure S4D). The data suggest a major role of MLN macrophages in initiating inflammation in *Angptl4*$^{-/-}$ mice fed HFD.

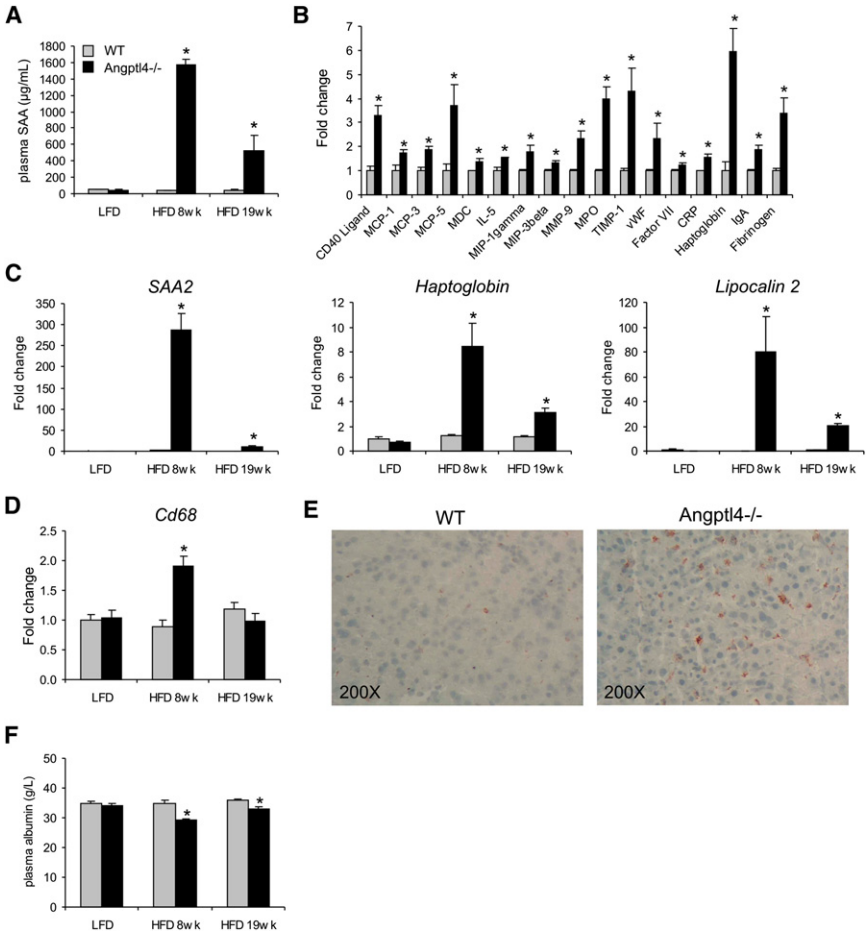

Figure 3. High-Fat Feeding Provokes Massive Acute Phase Response in *Angptl4*$^{-/-}$ Mice

(A) Plasma serum amyloid (SAA) levels in WT and *Angptl4*$^{-/-}$ mice fed LFD or HFD (study 1).

(B) Plasma levels of numerous cytokines in WT and *Angptl4*$^{-/-}$ fed HFD for 8 weeks. Values are expressed relative to WT.

(C) Hepatic mRNA levels of SAA2, haptoglobin, and lipocalin 2 determined by qPCR. Expression was normalized against 36B4.

(D) Hepatic mRNA levels of macrophage marker Cd68.

(E) Cd68 immunostaining of liver sections of WT and *Angptl4*$^{-/-}$ mice fed HFD for 8 weeks.

(F) Plasma serum albumin levels. n = 4–11 mice per group. Error bars represent SEM. Asterisk indicates significantly different from corresponding WT mice according to Student's t test ($p < 0.05$).

Previously, TG-rich VLDL particles were shown to stimulate foam cell formation and provoke release of cytokines by mouse peritoneal macrophages by serving as source of proinflammatory saturated fatty acids (Gianturco et al., 1982; Saraswathi and Hasty, 2006). This effect required LPL, which is highly expressed in macrophages (Babaev et al., 1999; Ostlund-Lindqvist et al., 1983; Skarlatos et al., 1993) and lymph nodes (http://biogps.gnf.org/) (Lattin et al., 2008). Microarray analysis indicated that LPL was among the top 25 of genes with the highest microarray expression signal in peritoneal mouse macrophages (Table S3). Since Angptl4 is also expressed in macrophages, is dramatically induced by chyle (Figure S5A), and can inhibit macrophage LPL (Figure S5B), we hypothesized that Angptl4 minimizes lipolysis of chylomicrons by MLN macrophages and accordingly suppresses uptake of proinflammatory saturated fatty acids. To test this hypothesis, peritoneal macrophages from *Angptl4*$^{-/-}$ mice were incubated with chyle obtained from the mesenteric lymph duct of rats fed palm oil-based HFD. Chyle dramatically increased lipid storage in macrophages leading to foam cell formation, which was strongly reduced by the LPL inhibitor orlistat (Figure S5C). Increased lipid uptake was verified by elevated expression of PPAR-LXR target *Abca1* and decreased expression of SREBP targets, as shown by whole genome expression profiling (Figure 6A) and qPCR (Figure S5D). Importantly, increased lipid uptake was associated with pronounced induction of numerous inflammation and immune-related genes, as shown by significant overrepresentation of GO classes corresponding to those pathways and by Ingenuity Canonical Pathway analysis (Figures S6A and S6B). Induction of inflammation, exemplified by *Cxcl2*, *Gdf15*, *oncostatin M*, *Ptgs2* (COX-2), and other genes, was almost entirely blunted by orlistat, indicating lipolysis and LPL dependency (Figure 6A). Some overlap in macrophage gene regulation was observed between chyle and LPS, but overall effects were mostly divergent (Figure S6C). Specifically, typical targets of LPS such as IL-1β were not induced by chyle, while numerous inflammatory genes upregulated by chyle were not induced by LPS, including *Gdf15* and *Vegfa*.

To examine whether Angptl4 can mimic the effect of orlistat on macrophage inflammation, macrophages were loaded with chyle in the presence of recombinant Angptl4. Angptl4 did not influence cell viability, which was equally high in Angptl4- and PBS-treated cells (>85%). At a concentration that causes maximal inhibition of LPL (Lichtenstein et al., 2007), Angptl4 prevented lipid uptake from chyle (Figure 6B) and markedly reduced inflammation (Figures 6A and 6C), as shown by strongly blunted induction of inflammatory markers *Ptgs2*, *Cxcl2*, *Ccr1*, and *Gdf15*. Inhibitory effects of Angptl4 and orlistat on chyle-elicited changes in inflammatory gene expression were highly similar and support a common mechanism of action (Figure 6A). No clear differences in foam cell formation upon chyle loading were observed between WT and *Angptl4*$^{-/-}$ macrophages (Figure S5C), likely because induction of Angptl4 protein by chyle in WT macrophages and subsequent feedback inhibition of lipid uptake via LPL lag behind the extremely rapid rate of lipid uptake.

Angptl4 Abolishes Chyle-Induced ER Stress in Macrophages

To explore the mechanism mediating the proinflammatory effect of chyle, peritoneal macrophages were incubated with different

chemical modulators including an inhibitor of LPS-induced TLR4 signaling (Polymyxin B), sphingolipid biosynthesis (Myriocin), and fatty acid translocase/Cd36 (Sulfosuccinimidyl oleate) (Figure 6D). None of the compounds showed any repressive effect on chyle-induced inflammation, although the LPS inhibitor polymyxin B augmented expression of *Gdf15* and *Cxcl2*.

Since ER stress was one of the canonical pathways significantly altered by chyle (Table S6B) and is linked to activation of inflammation (Hotamisligil, 2010), we further focused our investigation on the ER stress pathway. The mammalian ER stress pathway consists of three major branches: IRE1α, PERK, and ATF6. Upon ER stress activation, IRE1α and PERK undergo autophosphorylation and initiate downstream targets. IRE1α mediates the splicing of XBP1 mRNA, while PERK phosphorylates eIF2α, leading to attenuation of global translation and induction of expression of Atf4 and Ddit3 (CHOP). Remarkably, similar to the effect of ER stress inducers thapsigargin and tunicamycin, chyle significantly increased total IRE1α protein and IRE1α phosphorylation (Figure 7A) and dramatically stimulated XBP1 splicing (Figure 7B). Moreover, chyle stimulated phosphorylation of PERK and its target eIF2α, markedly increased CHOP protein, and upregulated expression of many ER stress target genes including *XBP1s*, *CHOP*, and *Atf4* (Figure 7C). Importantly and consistent with its antilipolytic role, effects of chyle on ER stress marker genes were entirely abolished by Angptl4 (Figure 7D). Taken together, chyle induces ER stress in macrophages, which may account for the pronounced activation of inflammation.

Saturated and Unsaturated Fatty Acids Differentially Modulate Angptl4 mRNA and ER Stress

As mentioned above, chyle dramatically increased *Angptl4* mRNA in WT peritoneal macrophages (Figure 7E). Similarly, individual fatty acids markedly increased *Angptl4* mRNA in mouse peritoneal and human U937 macrophages (Figure 7F). Compared to unsaturated oleic and linoleic acid, the saturated palmitic acid was significantly less potent in inducing *Angptl4*. In contrast, expression of *IRE1α*, *XBP1s*, *CHOP*, *Atf4*, and *Gdf15* and to a lesser extent *Cxcl2* was specifically stimulated by palmitic acid (Figure 7G). Palmitic, oleic, and linoleic acid represent 95% of fatty acids present in the various diets used, excluding the MCT diet.

Finally, to study which specific PPAR isotype is involved in Angptl4 regulation by fatty acids, three types of macrophages were treated with synthetic agonists for PPARα, PPARδ, and PPARγ. No induction of *Angptl4* expression was observed with PPARα agonist Wy14643 (Figure S7A). The PPARδ agonist GW501516 consistently induced *Angptl4* mRNA in all three cell types, whereas the PPARγ agonist rosiglitazone increased *Angptl4* mRNA in peritoneal macrophages and to a minor extent in U937 cells. These data suggest that PPARδ most likely mediates the effect of chylomicron-derived fatty acids on *Angptl4* expression.

Taken together, these results demonstrate that Angptl4 protects MLN macrophages from uncontrolled lipid accumulation after high-fat feeding, thereby preventing lipid-induced ER stress and consequent inflammation.

DISCUSSION

After a saturated fat-rich meal, MLNs are exposed to extremely high concentrations of chylomicrons via the chyle, which might lead to generation of large amounts of proinflammatory saturated fatty acids upon TG lipolysis. Our data indicate that MLNs and specifically resident macrophages are protected from the proinflammatory effect of saturated fatty acids via expression of Angptl4, which is strongly induced by chyle and fatty acids and which via inhibition of LPL prevents lipolysis of chylomicron-TG. In the absence of this protective autocrine mechanism, feeding a diet rich in saturated fat rapidly leads to enhanced lipid uptake into MLN-resident macrophages, triggering foam (Touton) cell formation and a massive inflammatory response characterized by severe mesenteric lymphadenitis. Concomitant induction of numerous cytokines leads to a massive hepatic acute phase response via the connecting portal circulation, further evolving into a progressive, uncontrolled inflammation that culminates in chylous ascites and fibrinopurulent peritonitis. The data thus show that Angptl4 is a key player in the protection against the severe proinflammatory effects of dietary saturated fat. Based on our data in mice, it can be hypothesized that human subjects homozygous for the E40K mutation in Angptl4, which has reduced ability to inhibit LPL and is associated with lower plasma TG (Romeo et al., 2007; Shan et al., 2008; Yin et al., 2009), may be particularly sensitive to the proinflammatory effects of dietary saturated fat.

According to microarray analysis, LPL was among the most highly expressed genes in mouse peritoneal macrophages. The ability of macrophage LPL to facilitate lipid uptake into macrophages is well recognized (Babaev et al., 1999; Ostlund-Lindqvist et al., 1983). The locally released fatty acids may serve as energy source for active macrophages (Yin et al., 1997), but may also constitute a potential proinflammatory stimulus. Consistent with this notion, fatty acids offered to macrophages as VLDL-TG are taken up and engage MAPK-mediated inflammatory pathways along with increased expression of several proinflammatory cytokines (Saraswathi and Hasty, 2006). Our data indicate that exposure of macrophages to elevated yet physiologically relevant concentrations of chylomicrons containing saturated fatty acids unleashes a vast inflammatory response characterized by marked induction of numerous chemokines and other inflammation-related genes, which is entirely dependent on TG-lipolysis. We propose that expression of Angptl4 in macrophages and its potent induction by chylomicron-derived fatty acids are part of a feedback mechanism aimed at protecting MLN-resident macrophages against postprandial lipid overload and associated inflammation.

Ablation of Angptl4 is associated with decreased plasma TG levels caused by increased peripheral LPL activity (Koster et al., 2005). Recent data indicate that endothelium-bound LPL is stabilized by the protein GPIHBP1, which partially prevents LPL inhibition by Angptl4 (Sonnenburg et al., 2009). Perhaps the almost complete blockage of lipid uptake by Angptl4 in macrophages as opposed to its more modest effect in muscle and adipose tissue may be explained by the minimal expression of GPIHBP1 in macrophages (Figure S7B) (Sonnenburg et al., 2009). Future studies will have to address this issue in more detail.

Feeding *Angptl4*$^{-/-}$ mice a diet rich in polyunsaturated fatty acids did not elicit an inflammatory response, consistent with data in peritoneal macrophages showing lack of induction of *Gdf15* and *Cxcl2* by oleic and linoleic acid. In contrast, oleic

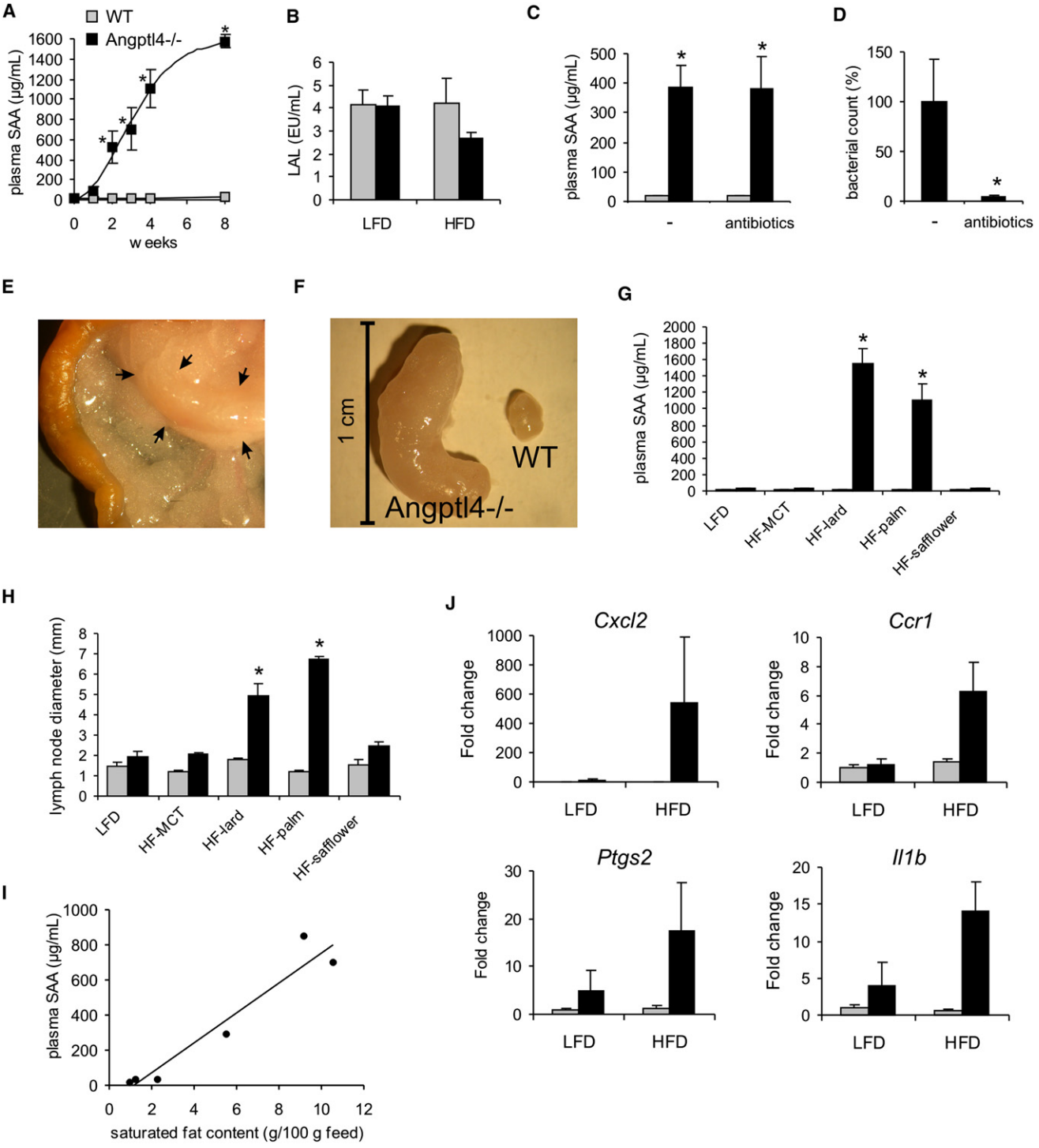

Figure 4. Chyle Containing Saturated Fat Elicits Massive Mesenteric Lymphadenitis in *Angptl4*$^{-/-}$ Mice

(A) Kinetics of change in plasma SAA in WT and *Angptl4*$^{-/-}$ mice fed HFD. n = 6–7 per group.

(B) Postprandial endotoxin levels in portal plasma from WT and *Angptl4*$^{-/-}$ mice fed LFD or HFD for 5 weeks (study 2). n = 6–7 per group.

(C) Plasma SAA levels in WT and *Angptl4*$^{-/-}$ mice fed HFD for 5 weeks being given oral antibiotics or vehicle (study 3). n = 6–10 per group.

(D) Relative abundance of total bacteria expressed per weight of colonic content in *Angptl4*$^{-/-}$ mice fed HFD and given oral antibiotics or vehicle. Asterisk indicates significantly different from corresponding WT mice according to Student's t test ($p < 0.05$).

(E) Photograph of mesenteric fat of *Angptl4*$^{-/-}$ mouse fed HFD for 5 weeks (study 2). Position of dramatically enlarged lymph node is indicated.

(F) MLN of WT and *Angptl4*$^{-/-}$ mice fed HFD for 5 weeks after dissection and removal of adipose tissue.

(G) Plasma SAA levels in WT and *Angptl4*$^{-/-}$ mice fed LFD or different types of HFD for 5 weeks (study 2). HF-MCT, high-fat medium-chain triglycerides; HF-lard, high-fat lard-based; HF-palm, high-fat palm oil-based; HF-safflower, high-fat safflower oil-based.

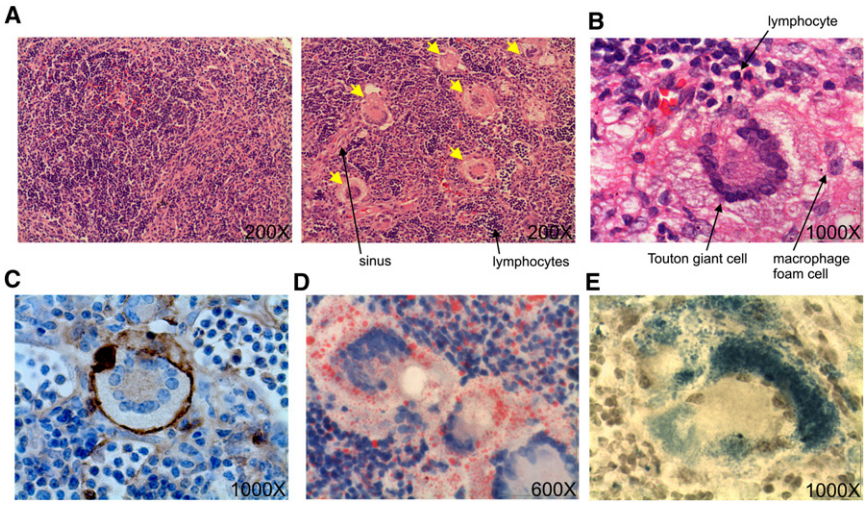

Figure 5. Touton Giant Cells Are Abundant in MLN of *Angptl4*$^{-/-}$ Mice Fed HFD

(A) Low-magnification image of H&E staining of MLN from WT and *Angptl4*$^{-/-}$ mice fed HFD for 5 weeks (study 2). Touton giant cells are indicated by yellow arrows. (B) High-magnification image of MLN with Touton giant cells from *Angptl4*$^{-/-}$ mice fed HFD for 5 weeks (C) F4/80 immunostaining of MLN with Touton giant cell. (D) Oil red O staining counterstained with hematoxylin. (E) Sudan black staining.

and linoleic acid were much more potent inducers of Angptl4 expression compared to palmitic acid, suggesting that the Angptl4-mediated feedback inhibition of lipid uptake and inflammation is disturbed in presence of saturated fatty acids.

An important question is how chyle induces inflammation in macrophages. Use of chemical inhibitors indicated that the response is not mediated by LPS, is not dependent on Cd36-mediated fatty acid transport, and does not require sphingolipid synthesis. Strikingly, chyle caused pronounced activation of different branches of the ER stress pathway. It has been shown that ER stress can promote inflammation by various mechanisms, including via IRE1α-mediated activation of stress kinases such as the c-Jun N-terminal kinase (Urano et al., 2000), and via PERK-mediated activation of NF-κB (Jiang et al., 2003). We found that chyle stimulated IRE1α phosphorylation to promote XBP1 splicing, and activated PERK, eIF2α, and their downstream targets. Activation of ER stress in peritoneal macrophages could be reproduced by free palmitic acid but not oleic or linoleic acid, suggesting the response is mediated by saturated fatty acids.

The mechanism by which saturated fatty acids induce ER stress has been the subject of recent investigations. Palmitate but not palmitoleate induced ER stress in pancreatic β cells (Diakogiannaki et al., 2008). In liver cells saturated fatty acids induced ER stress independently of ceramide synthesis (Wei et al., 2006). Stimulation of ER stress by palmitate may occur via increasing the saturated lipid content of ER membrane phospholipids and TG, leading to compromised ER morphology and integrity and impaired function of protein-folding chaperones (Borradaile et al., 2006). Data also point to an important role for aP2 (Fabp4) in linking saturated fatty acids to ER stress in macrophages via alterations in lipid composition (Erbay et al., 2009).

Several studies have attributed the proinflammatory effect of saturated fatty acids to activation of TLR4 (Lee et al., 2001; Shi et al., 2006; Suganami et al., 2007). Recently, interplay between TLR4 (and TLR2) and the ER stress pathway was demonstrated (Woo et al., 2009). IRE1α was shown to be a positive regulator of the inflammatory response to TLR activation in macrophages, while the PERK pathway was not induced by TLR signaling (Martinon et al., 2010). These data hint at a possible role for TLR signaling in the response to chyle in macrophages. However, unlike TLR signaling, chyle dramatically induced ER stress, as evidenced by the activation of ER stress sensors IRE1α and PERK as well as their downstream targets. Additionally, whole-genome analysis of gene regulation by chyle versus LPS revealed some overlap, but chyle clearly did not mimic LPS, as illustrated by the differential response of classic LPS/TLR4-target IL-1β. Although these data do not rule out a role for TLR signaling in mediating the inflammatory effects of chyle, induction of ER stress seems a much more plausible mechanism.

A previous report briefly alluded to development of chylous ascites in *Angptl4*$^{-/-}$ mice after 20 weeks of HFD (Desai et al., 2007). In that study it was found that repeated injections of WT mice fed HFD with a monoclonal antibody against Angptl4 recapitulated the phenotype of *Angptl4*$^{-/-}$ mice. Since the antibody is directed against the N-terminal portion of Angptl4 and abolishes its ability to inhibit LPL, the data support the notion that the clinical abnormalities in *Angptl4*$^{-/-}$ mice fed HFD are related to altered LPL activity, and are independent of C-terminal Angptl4.

Chylous ascites has been observed in mice heterozygous for the transcription factor Prox1 as well as in mice lacking Angiopoietin-2. Both proteins are essential for development of the lymphatic vasculature (Gale et al., 2002; Harvey et al., 2005). Accordingly, it is tempting to hypothesize a similar role for Angptl4. However, *Prox1*$^{+/-}$ and *Angiopoietin2*$^{-/-}$ mice develop chylous ascites shortly after birth, reflecting a severe developmental defect. In contrast, *Angptl4*$^{-/-}$ mice do not exhibit ascites unless challenged with HFD for at least 12 weeks. Rather, the data indicate that ascites was secondary to progressive inflammation originating in MLN macrophages, leading to massive lymphadenitis and consequent obstruction in mesenteric lymph flow, which in turn caused dilation of intestinal

(H) Size of MLN in WT and *Angptl4*$^{-/-}$ mice fed LFD or different types of HFD for 5 weeks. n = 6–7 mice per group. Means of *Angptl4*$^{-/-}$ mice fed HF-palm or HF-lard were significantly different from the other groups as determined by one-way ANOVA followed by Tukey's post-hoc test.

(I) Close correlation between saturated fat content of the diet and the mean plasma level of SAA in *Angptl4*$^{-/-}$ mice after 3 weeks of feeding.

(J) Expression of inflammatory marker genes in MLN of WT and *Angptl4*$^{-/-}$ mice fed HFD for 24 hr (study 4). n = 3 per group. Error bars represent SEM.

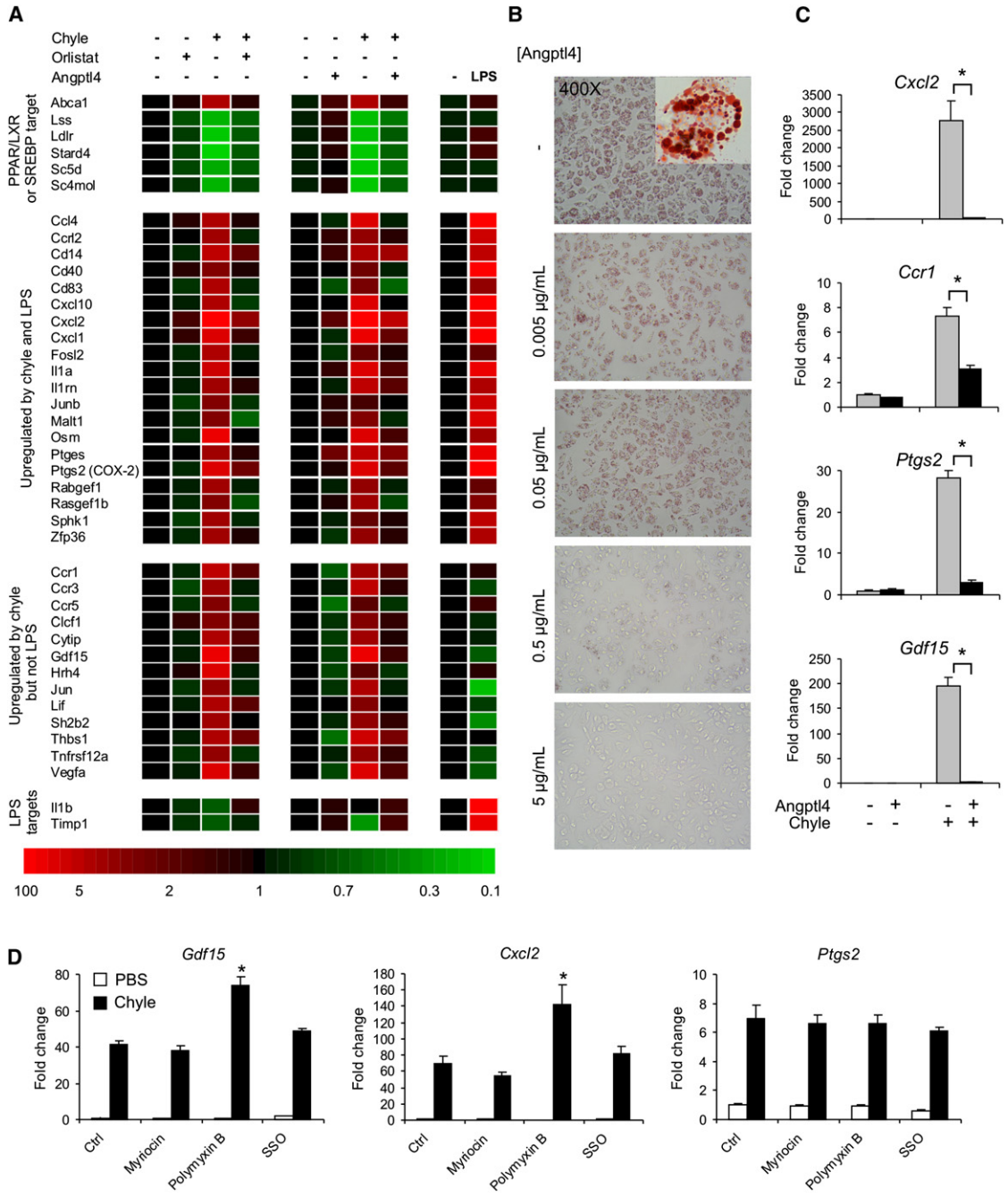

Figure 6. Angptl4 Inhibits Macrophage Foam Cell Formation and Inflammatory Gene Expression

(A) Heat map showing changes in expression of selected genes in *Angptl4*$^{-/-}$ mouse peritoneal macrophages incubated for 6 hr with chyle (final TG concentration 2 mM) and/or orlistat (20 μM), or with chyle and/or recombinant Angptl4 (2.5 μg/mL). Expression in untreated macrophages was set at 1. In parallel, expression changes are shown of same genes in peritoneal macrophages treated for 4 hr with LPS (100 ng/mL). All genes induced by chyle by at least 2.5-fold and which are labeled with "cytokine or chemokine activity" or "immune or inflammatory response" by Gene Ontology (Biological Process) or are involved in immunity/inflammation based on literature study were included. Also, SREBP target genes that were >75% suppressed by chyle were included.

(B) Oil red O staining of *Angptl4*$^{-/-}$ mouse peritoneal macrophages incubated for 6 hr with chyle (TG concentration 2 mM) and increasing concentrations of mouse recombinant Angptl4. Chyle was collected from rats fed palm oil-based HFD. (Inset) High-magnification image of macrophage foam cell.

(C) Q-PCR expression of inflammatory genes in *Angptl4*$^{-/-}$ macrophages treated with chyle and/or Angptl4 (2.5 μg/mL). Asterisk indicates significantly different according to Student's t test ($p < 0.05$).

(D) Q-PCR expression of inflammatory genes in *Angptl4*$^{-/-}$ macrophages treated with chyle and various pharmacologic inhibitors. SSO, sulfosuccinimidyl oleate. Differences were evaluated for statistical significance by one-way ANOVA followed by Tukey's post-hoc test. Asterisk indicates significantly different from control-treated cells ($p < 0.05$). Error bars represent SEM.

lymphatic vessels. Furthermore, inflammation of MLN and mesenteric fat led to increased local lymphatic and vascular permeability, as shown by chylous ascites and low SAAG, respectively, which is indicative of exudative ascites. The more than 2-fold higher protein concentration in ascites fluid compared to chyle supports an important contribution of vascular leakage next to leakage from chyle. Increased circulatory leakage caused fibrinogen extravasation, which after clotting accumulated as fibrin and covered abdominal organs. Chronic inflammation likely gave rise to impaired intestinal barriers function and translocation of enteric bacteria, causing peritonitis and death of the animals.

In conclusion, Angptl4 protects against the severe proinflammatory effects of dietary saturated fat in MLN by inhibiting macrophage LPL, thereby reducing lipolytic release of fatty acids, macrophage foam cell formation, ER stress, and initiation of a marked inflammatory response. The data illustrate how the unique anatomy of the intestinal lymphatic system in which immune cells residing in MLN are exposed to excessive postprandial TG concentrations requires activation of an effective cellular mechanism that protects against elevated lipid uptake and its complications. It can be speculated that the inability to effectively recruit this mechanism may contribute to proinflammatory changes related to elevated saturated fat consumption.

EXPERIMENTAL PROCEDURES

Animals

Animal studies were done using pure-bred WT and *Angptl4*$^{-/-}$ mice on C57Bl/6 background (Koster et al., 2005). In study 1, male 11-week-old mice were fed LFD or HFD for 8 or 19 weeks, providing 10% or 45% energy percent as TG (D12450B or D12451, Research Diets, Inc., Table S1) (Research Diets Services, Wijk bij Duurstede, Netherlands), after 3 week run in (adaptation period) with LFD. In study 2, male 10- to 18-week-old mice were fed LFD or HFD for 5 weeks, after 2 week run in with LFD. Fat source of the HFD was either palm oil (standard HFD used in studies 1, 3, and 4, Table S1), lard, MCT oil, or safflower oil (Table S2). Blood was collected from tail vein at weekly intervals. In study 3, male 12-week-old mice were fed standard HFD for 5 weeks, after 2 week run in with standardized LFD AIN93G (see http://testdiet.purina-mills.com/PDF/57W5.pdf and Table S2). The following antibiotics were provided in drinking water: ampicillin (1 g/L), neomycin (1 g/L), and metronidazole (0.5 g/L). Blood was collected from tail vein at weekly intervals. In study 4, mice were fed low-fat AIN93G or standard HFD for 24 hr, after 1 week run in with AIN93G. In the latter studies, low-fat AIN93G was chosen instead of D12450B to achieve minimal dietary saturated fat intake. Diet composition is provided in Tables S1 and S2. At the end of each study, mice were anaesthetized with mixture of isoflurane (1.5%), nitrous oxide (70%), and oxygen (30%). Blood was collected by orbital puncture into EDTA tubes. Mice were killed by cervical dislocation, after which tissues were excised and directly frozen in liquid nitrogen or prepared for histology.

Wistar rats were fed palm oil-based HFD (D12451) overnight. The next morning, animals were anesthetized using isoflurane, and mesenteric lymph ducts were cannulated. Chyle was collected for 1–2 hr and stored at −20°C. Chyle TG concentrations averaged at 35 ± 11 mM as determined by enzymatic assay (Instruchemie, Delfzijl, Netherlands). Animal studies were approved by the local animal ethics committee at Wageningen University.

Two terminally ill animals were transferred to the Small Animal Pathology laboratory of the Faculty of Veterinary Medicine at Utrecht University for formal autopsy by a licensed animal pathologist.

Cell Culture

U937 human monocytes were differentiated into macrophages by 24 hr treatment with phorbol myristate acetate (10 ng/μL). U937 macrophages were subsequently incubated for 6 hr with fatty acids (C16:0, C18:1, C18:2) coupled to fatty acid free BSA to a final concentration of 500 μM as previously described (de Vogel-van den Bosch et al., 2008).

To obtain peritoneal macrophages, WT and *Angptl4*$^{-/-}$ mice were injected intraperitoneally with 1 ml 4% thioglycollate. Three days later, animals were anesthesized with isoflurane, bled via orbital puncture, and peritoneal cavities washed using 10 ml ice-cold RPMI medium supplemented with 100 U/mL penicillin and 100 μg/mL streptomycin (Lonza, Verviers, Belgium). Cell pellets were incubated with RBC lysis buffer on ice for 5 min and subsequently washed with RPMI medium supplemented with 10% fetal bovine serum (FBS) (Lonza) and antibiotics, repelletized, and seeded at density of 3×10^5 cells/cm^2. Two hours later, cells were washed twice with PBS to remove non-adherent cells and provided with medium. Two days later, cells were exposed to chyle at TG concentration of 2 mM for 6 hr preceded by preincubation with 20 μM orlistat (Sigma Zwijndrecht, Netherlands) or 2.5 μg/mL mouse recombinant Angptl4 (R&D Systems, Abingdon, UK) for 1.5 hr. To explore the mechanism induced by chyle, *Angptl4*$^{-/-}$ macrophages were preincubated with 10 μM myriocin, 10 μg/ml Polymyxin B, or 0.5 mM Sulfosuccinimidyl oleate (SSO) for 30 min followed by exposure of cells to either PBS or chyle at TG concentration of 2 mM for 6 hr. In ER stress experiments, *Angptl4*$^{-/-}$ macrophages were exposed to 100 nM thapsigargin, 2.5 μg/ml tunicamycin, or chyle (TG 2 mM) for 6 hr. Analysis of ER stress in peritoneal macrophages was carried out as described (Yang et al., 2010).

Histology/Immunohistochemistry

Hematoxylin and eosin (H&E) staining of sections was performed using standard protocols. For detection of macrophages, immunohistochemistry was performed using antibody against Cd68 (liver, adipose tissue) or F4/80 (lymph nodes) (Serotec, Oxford, UK). Paraffin-embedded sections were preincubated with 20% normal goat serum followed by overnight incubation at 4°C with primary antibody diluted 1:50 in PBS/1% BSA. After incubation with primary antibody, goat anti-rat IgG conjugated to horseradish peroxidase (Serotec) was used as secondary antibody. Visualization was performed using AEC Substrate Chromogen (Cd68) or 3,3′-diaminobenzidine (F4/80). Negative controls were prepared by omitting primary antibody.

For Sirius red staining, paraffin-embedded sections of small intestine were mounted on Superfrost microscope slides. Sections were dewaxed in xylene and rehydrated in series of graded alcohols. Slides were stained in picrosirius red 0.1% picric acid for 90 min and rinsed in acidified H_2O 0.5% acetic acid.

Oil red O stock solution was prepared by dissolving 0.5 g oil red O (Sigma, #O0625) in 500 ml isopropanol. Oil red O working solution was prepared by mixing 30 ml oil red O stock with 20 ml dH_2O, followed by filtration. Sections (5 μm) were cut from frozen MLNs embedded in OCT. Sections were air dried for 30 min, rehydrated in dH_2O, and fixated for 10 min in formal calcium (4% formaldehyde, 1% $CaCl_2$). Sections were immersed in oil red O working solution for 10 min, followed by two rinses with dH_2O. Hematoxylin nuclei staining was subsequently carried out for 5 min followed by several rinses with dH_2O. Sections were mounted in aqueous mountant (Imsol, Preston, UK).

For Sudan black staining, 0.5 g Sudan black (Sigma, #86015) was dissolved in 100 ml warm 70% ethanol and subsequently filtered. Sections were fixed and rehydrated as above. After two 3 min rinses with 50% ethanol and two quick rinses with dH_2O, sections were immersed in Sudan black solution for 10 min, followed by two rinses with dH_2O. Sections were mounted in aqueous mountant (Imsol, Preston, UK).

SUPPLEMENTAL INFORMATION

Supplemental Information includes seven figures, three tables, Supplemental Experimental Procedures, and Supplemental References and can be found with this article online at doi:10.1016/j.cmet.2010.11.002.

ACKNOWLEDGMENTS

We thank Shohreh Keshtkar, Karin Mudde, Jenny Jansen, Mechteld Grootte-Bromhaar, Rinke Stienstra, and Els Oosterink for laboratory analyses; Dr. Ben Witteman for clinical consultations; and Dr. Mark Boekschoten for assistance with microarray analysis. This work was supported by Nutrigenomics Consortium, TI Food and Nutrition, Netherlands Heart Foundation (2007B046), Netherlands Organisation for Scientific Research (40-00812-98-08030),

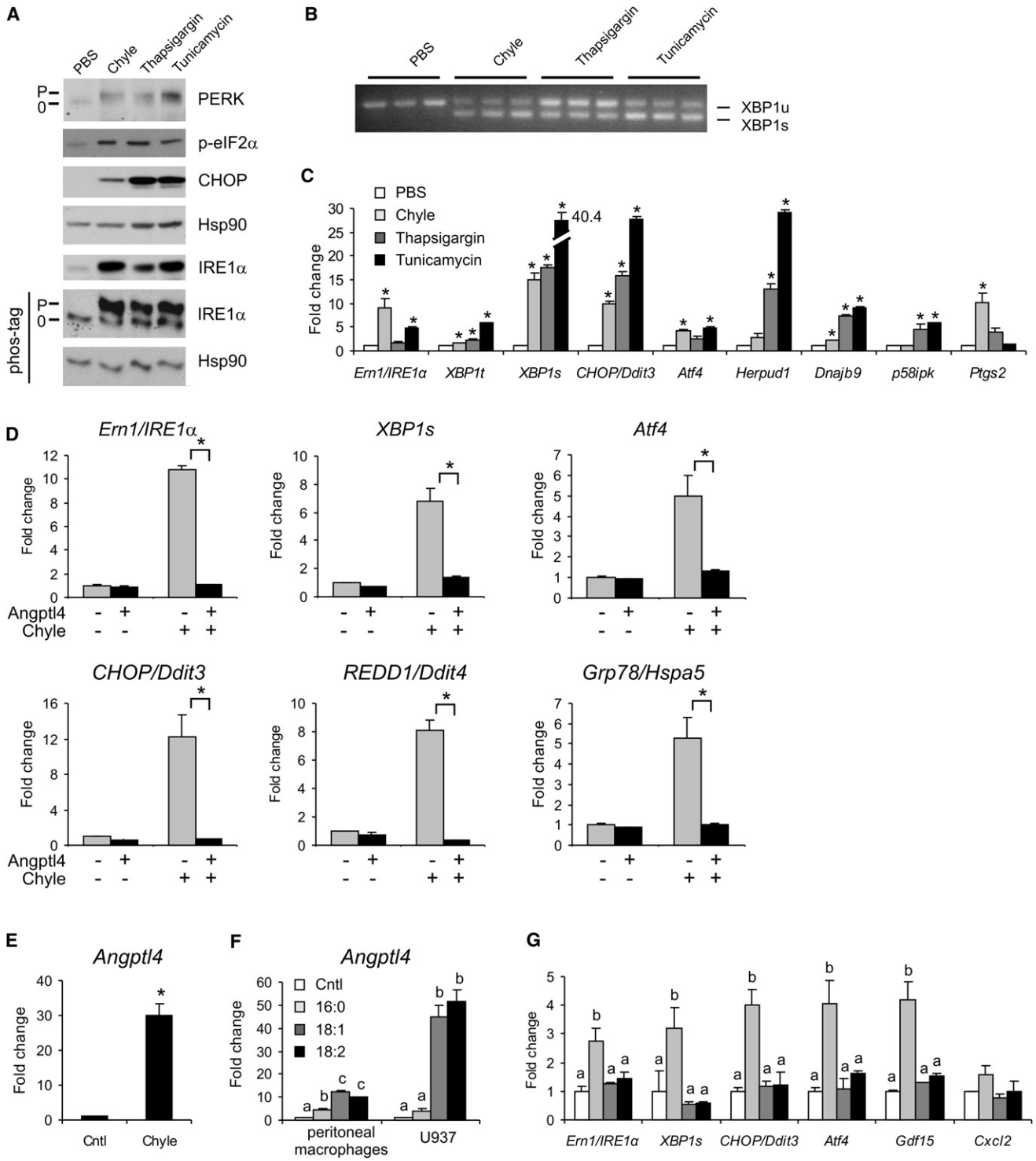

Figure 7. Angptl4 Prevents Chyle-Induced ER Stress

(A) Immunoblots of IRE1α, PERK, eIF2α, and CHOP using regular gels or Phos-tag gels (IRE1α only) of *Angptl4*$^{-/-}$ macrophages treated with chyle (TG concentration 2 mM), thapsigargin (100 nM), or tunicamycin (2.5 μg/mL) for 6 hr. "P" represents phosphorylated form.

(B) Regular RT-PCR of XBP1 processing revealing spliced and unspliced XBP1 mRNA.

(C) Q-PCR expression of ER stress genes. Differences were evaluated for statistical significance by one-way ANOVA followed by Tukey's post-hoc test. Asterisk indicates significantly different from control-treated cells ($p < 0.05$).

(D) Q-PCR expression of selected genes involved in ER stress in *Angptl4*$^{-/-}$ mouse peritoneal macrophages incubated for 6 hr with chyle and/or recombinant Angptl4 (2.5 μg/mL). Asterisk indicates significantly different according to Student's t test ($p < 0.05$).

National Institutes of Health (R01DK082582), and American Diabetes Association 7-08-JF-47. L.L., F.M., N.J.d.W., G.J.H., Y.H., and S.K. collected experimental data. L.L., F.M., N.J.d.W., G.J.H., R.v.d.M., Y.H., L.Q., A.K., J.T.T., N.S.T., M.M., and S.K. participated in the design and interpretation of the study. L.L. and S.K. wrote the initial draft of the manuscript, which was corrected and approved by all authors.

Received: April 22, 2010
Revised: August 12, 2010
Accepted: September 9, 2010
Published: November 30, 2010

REFERENCES

Aterman, K., Remmele, W., and Smith, M. (1988). Karl Touton and his "xanthelasmatic giant cell." A selective review of multinucleated giant cells. Am. J. Dermatopathol. *10*, 257–269.

Babaev, V.R., Fazio, S., Gleaves, L.A., Carter, K.J., Semenkovich, C.F., and Linton, M.F. (1999). Macrophage lipoprotein lipase promotes foam cell formation and atherosclerosis in vivo. J. Clin. Invest. *103*, 1697–1705.

Backhed, F., Crawford, P.A., O'Donnell, D., and Gordon, J.I. (2007). Postnatal lymphatic partitioning from the blood vasculature in the small intestine requires fasting-induced adipose factor. Proc. Natl. Acad. Sci. USA *104*, 606–611.

Borradaile, N.M., Han, X., Harp, J.D., Gale, S.E., Ory, D.S., and Schaffer, J.E. (2006). Disruption of endoplasmic reticulum structure and integrity in lipotoxic cell death. J. Lipid Res. *47*, 2726–2737.

Cani, P.D., Amar, J., Iglesias, M.A., Poggi, M., Knauf, C., Bastelica, D., Neyrinck, A.M., Fava, F., Tuohy, K.M., Chabo, C., et al. (2007). Metabolic endotoxemia initiates obesity and insulin resistance. Diabetes *56*, 1761–1772.

Desai, U., Lee, E.C., Chung, K., Gao, C., Gay, J., Key, B., Hansen, G., Machajewski, D., Platt, K.A., Sands, A.T., et al. (2007). Lipid-lowering effects of anti-angiopoietin-like 4 antibody recapitulate the lipid phenotype found in angiopoietin-like 4 knockout mice. Proc. Natl. Acad. Sci. USA *104*, 11766–11771.

de Vogel-van den Bosch, H.M., de Wit, N.J., Hooiveld, G.J., Vermeulen, H., van der Veen, J.N., Houten, S.M., Kuipers, F., Muller, M., and van der Meer, R. (2008). A cholesterol-free, high-fat diet suppresses gene expression of cholesterol transporters in murine small intestine. Am. J. Physiol. Gastrointest. Liver Physiol. *294*, G1171–G1180.

Diakogiannaki, E., Welters, H.J., and Morgan, N.G. (2008). Differential regulation of the endoplasmic reticulum stress response in pancreatic beta-cells exposed to long-chain saturated and monounsaturated fatty acids. J. Endocrinol. *197*, 553–563.

Erbay, E., Babaev, V.R., Mayers, J.R., Makowski, L., Charles, K.N., Snitow, M.E., Fazio, S., Wiest, M.M., Watkins, S.M., Linton, M.F., et al. (2009). Reducing endoplasmic reticulum stress through a macrophage lipid chaperone alleviates atherosclerosis. Nat. Med. *15*, 1383–1391.

Gale, N.W., Thurston, G., Hackett, S.F., Renard, R., Wang, Q., McClain, J., Martin, C., Witte, C., Witte, M.H., Jackson, D., et al. (2002). Angiopoietin-2 is required for postnatal angiogenesis and lymphatic patterning, and only the latter role is rescued by Angiopoietin-1. Dev. Cell *3*, 411–423.

Gianturco, S.H., Bradley, W.A., Gotto, A.M., Jr., Morrisett, J.D., and Peavy, D.L. (1982). Hypertriglyceridemic very low density lipoproteins induce triglyceride synthesis and accumulation in mouse peritoneal macrophages. J. Clin. Invest. *70*, 168–178.

Harvey, N.L., Srinivasan, R.S., Dillard, M.E., Johnson, N.C., Witte, M.H., Boyd, K., Sleeman, M.W., and Oliver, G. (2005). Lymphatic vascular defects promoted by Prox1 haploinsufficiency cause adult-onset obesity. Nat. Genet. *37*, 1072–1081.

Hotamisligil, G.S. (2010). Endoplasmic reticulum stress and the inflammatory basis of metabolic disease. Cell *140*, 900–917.

Jiang, H.Y., Wek, S.A., McGrath, B.C., Scheuner, D., Kaufman, R.J., Cavener, D.R., and Wek, R.C. (2003). Phosphorylation of the alpha subunit of eukaryotic initiation factor 2 is required for activation of NF-kappaB in response to diverse cellular stresses. Mol. Cell. Biol. *23*, 5651–5663.

Kersten, S., Mandard, S., Tan, N.S., Escher, P., Metzger, D., Chambon, P., Gonzalez, F.J., Desvergne, B., and Wahli, W. (2000). Characterization of the fasting-induced adipose factor FIAF, a novel peroxisome proliferator-activated receptor target gene. J. Biol. Chem. *275*, 28488–28493.

Koster, A., Chao, Y.B., Mosior, M., Ford, A., Gonzalez-DeWhitt, P.A., Hale, J.E., Li, D., Qiu, Y., Fraser, C.C., Yang, D.D., et al. (2005). Transgenic angiopoietin-like (angptl)4 overexpression and targeted disruption of angptl4 and angptl3: regulation of triglyceride metabolism. Endocrinology *146*, 4943–4950.

Lattin, J.E., Schroder, K., Su, A.I., Walker, J.R., Zhang, J., Wiltshire, T., Saijo, K., Glass, C.K., Hume, D.A., Kellie, S., et al. (2008). Expression analysis of G Protein-Coupled Receptors in mouse macrophages. Immunome Res. *4*, 5.

Lee, J.Y., Sohn, K.H., Rhee, S.H., and Hwang, D. (2001). Saturated fatty acids, but not unsaturated fatty acids, induce the expression of cyclooxygenase-2 mediated through Toll-like receptor 4. J. Biol. Chem. *276*, 16683–16689.

Lichtenstein, L., Berbee, J.F., van Dijk, S.J., van Dijk, K.W., Bensadoun, A., Kema, I.P., Voshol, P.J., Muller, M., Rensen, P.C., and Kersten, S. (2007). Angptl4 upregulates cholesterol synthesis in liver via inhibition of LPL- and HL-dependent hepatic cholesterol uptake. Arterioscler. Thromb. Vasc. Biol. *27*, 2420–2427.

Mandard, S., Zandbergen, F., van Straten, E., Wahli, W., Kuipers, F., Muller, M., and Kersten, S. (2006). The fasting-induced adipose factor/angiopoietin-like protein 4 is physically associated with lipoproteins and governs plasma lipid levels and adiposity. J. Biol. Chem. *281*, 934–944.

Martinon, F., Chen, X., Lee, A.H., and Glimcher, L.H. (2010). TLR activation of the transcription factor XBP1 regulates innate immune responses in macrophages. Nat. Immunol. *11*, 411–418.

Merkel, M., Eckel, R.H., and Goldberg, I.J. (2002). Lipoprotein lipase: genetics, lipid uptake, and regulation. J. Lipid Res. *43*, 1997–2006.

Oike, Y., Akao, M., Yasunaga, K., Yamauchi, T., Morisada, T., Ito, Y., Urano, T., Kimura, Y., Kubota, Y., Maekawa, H., et al. (2005). Angiopoietin-related growth factor antagonizes obesity and insulin resistance. Nat. Med. *11*, 400–408.

Ostlund-Lindqvist, A.M., Gustafson, S., Lindqvist, P., Witztum, J.L., and Little, J.A. (1983). Uptake and degradation of human chylomicrons by macrophages in culture. Role of lipoprotein lipase. Arteriosclerosis *3*, 433–440.

Romeo, S., Pennacchio, L.A., Fu, Y., Boerwinkle, E., Tybjaerg-Hansen, A., Hobbs, H.H., and Cohen, J.C. (2007). Population-based resequencing of ANGPTL4 uncovers variations that reduce triglycerides and increase HDL. Nat. Genet. *39*, 513–516.

Saraswathi, V., and Hasty, A.H. (2006). The role of lipolysis in mediating the proinflammatory effects of very low density lipoproteins in mouse peritoneal macrophages. J. Lipid Res. *47*, 1406–1415.

Shan, L., Yu, X.C., Liu, Z., Hu, Y., Sturgis, L.T., Miranda, M.L., and Liu, Q. (2008). The angiopoietin-like proteins ANGPTL3 and ANGPTL4 inhibit lipoprotein lipase activity through distinct mechanisms. J. Biol. Chem. *284*, 1419–1424.

Shi, H., Kokoeva, M.V., Inouye, K., Tzameli, I., Yin, H., and Flier, J.S. (2006). TLR4 links innate immunity and fatty acid-induced insulin resistance. J. Clin. Invest. *116*, 3015–3025.

(E) Angptl4 mRNA expression in WT mouse peritoneal macrophages treated for 6 hr with chyle (TG concentration 1.3 mM).
(F) Angptl4 mRNA expression in WT mouse peritoneal macrophages or human U937 macrophages treated for 6 hr with albumin-bound free fatty acids (500 μM).
(G) Q-PCR expression of selected genes in WT mouse peritoneal macrophages treated with albumin-bound free fatty acids (500 μM). Control cells were treated with albumin only. Differences were evaluated for statistical significance by one-way ANOVA followed by Tukey's post-hoc test. Bars with different letters are significantly different ($p < 0.05$). Error bars represent SEM.

Skarlatos, S.I., Dichek, H.L., Fojo, S.S., Brewer, H.B., and Kruth, H.S. (1993). Absence of triglyceride accumulation in lipoprotein lipase-deficient human monocyte-macrophages incubated with human very low density lipoprotein. J. Clin. Endocrinol. Metab. *76*, 793–796.

Sonnenburg, W.K., Yu, D., Lee, E.C., Xiong, W., Gololobov, G., Key, B., Gay, J., Wilganowski, N., Hu, Y., Zhao, S., et al. (2009). GPIHBP1 stabilizes lipoprotein lipase and prevents its inhibition by angiopoietin-like 3 and angiopoietin-like 4. J. Lipid Res. *50*, 2421–2429.

Suganami, T., Tanimoto-Koyama, K., Nishida, J., Itoh, M., Yuan, X., Mizuarai, S., Kotani, H., Yamaoka, S., Miyake, K., Aoe, S., et al. (2007). Role of the Toll-like receptor 4/NF-kappaB pathway in saturated fatty acid-induced inflammatory changes in the interaction between adipocytes and macrophages. Arterioscler. Thromb. Vasc. Biol. *27*, 84–91.

Tabata, M., Kadomatsu, T., Fukuhara, S., Miyata, K., Ito, Y., Endo, M., Urano, T., Zhu, H.J., Tsukano, H., Tazume, H., et al. (2009). Angiopoietin-like protein 2 promotes chronic adipose tissue inflammation and obesity-related systemic insulin resistance. Cell Metab. *10*, 178–188.

Urano, F., Wang, X., Bertolotti, A., Zhang, Y., Chung, P., Harding, H.P., and Ron, D. (2000). Coupling of stress in the ER to activation of JNK protein kinases by transmembrane protein kinase IRE1. Science *287*, 664–666.

Voshol, P.J., Rensen, P.C., van Dijk, K.W., Romijn, J.A., and Havekes, L.M. (2009). Effect of plasma triglyceride metabolism on lipid storage in adipose tissue: studies using genetically engineered mouse models. Biochim. Biophys. Acta *1791*, 479–485.

Wang, H., and Eckel, R.H. (2009). Lipoprotein lipase: from gene to obesity. Am. J. Physiol. Endocrinol. Metab. *297*, E271–E288.

Wei, Y., Wang, D., Topczewski, F., and Pagliassotti, M.J. (2006). Saturated fatty acids induce endoplasmic reticulum stress and apoptosis independently of ceramide in liver cells. Am. J. Physiol. Endocrinol. Metab. *291*, E275–E281.

Woo, C.W., Cui, D., Arellano, J., Dorweiler, B., Harding, H., Fitzgerald, K.A., Ron, D., and Tabas, I. (2009). Adaptive suppression of the ATF4-CHOP branch of the unfolded protein response by toll-like receptor signalling. Nat. Cell Biol. *11*, 1473–1480.

Xu, A., Lam, M.C., Chan, K.W., Wang, Y., Zhang, J., Hoo, R.L., Xu, J.Y., Chen, B., Chow, W.S., Tso, A.W., et al. (2005). Angiopoietin-like protein 4 decreases blood glucose and improves glucose tolerance but induces hyperlipidemia and hepatic steatosis in mice. Proc. Natl. Acad. Sci. USA *102*, 6086–6091.

Yang, L., Xue, Z., He, Y., Sun, S., Chen, H., and Qi, L. (2010). A Phos-tag-based approach reveals the extent of physiological endoplasmic reticulum stress. PLoS ONE *5*, e11621. 10.1371/journal.pone.0011621.

Yin, B., Loike, J.D., Kako, Y., Weinstock, P.H., Breslow, J.L., Silverstein, S.C., and Goldberg, I.J. (1997). Lipoprotein lipase regulates Fc receptor-mediated phagocytosis by macrophages maintained in glucose-deficient medium. J. Clin. Invest. *100*, 649–657.

Yin, W., Romeo, S., Chang, S., Grishin, N.V., Hobbs, H.H., and Cohen, J.C. (2009). Genetic variation in ANGPTL4 provides insights into protein processing and function. J. Biol. Chem. *284*, 13213–13222.

Yoon, J.C., Chickering, T.W., Rosen, E.D., Dussault, B., Qin, Y., Soukas, A., Friedman, J.M., Holmes, W.E., and Spiegelman, B.M. (2000). Peroxisome proliferator-activated receptor gamma target gene encoding a novel angiopoietin-related protein associated with adipose differentiation. Mol. Cell. Biol. *20*, 5343–5349.

Yoshida, K., Shimizugawa, T., Ono, M., and Furukawa, H. (2002). Angiopoietin-like protein 4 is a potent hyperlipidemia-inducing factor in mice and inhibitor of lipoprotein lipase. J. Lipid Res. *43*, 1770–1772.